Dalton Transactions

Activating the oxygen electrocatalytic activity of layer-structured Ca0.5CoO2 nanofibers by iron doping

Journal:	*Dalton Transactions*
Manuscript ID	DT-ART-11-2021-003883.R1
Article Type:	Paper
Date Submitted by the Author:	07-Jan-2022
Complete List of Authors:	Li, Mingyu; Jilin University Zhao, Bote; South China University of Technology Zhao, Yun; South China University of Technology Chen, Yu; South China University of Technology, School of Environment and Energy Liu, Meilin; Georgia Institute of Technology, School of Materials Science and Engineering

ARTICLE

Activating the oxygen electrocatalytic activity of layer-structured $Ca_{0.5}CoO_2$ nanofibers by iron doping

Mingyu Li,[a, b, c] Bote Zhao,*[c, d] Yun Zhao,[d] Yu Chen[d] and Meilin Liu*[c]

Received 00th January 20xx,
Accepted 00th January 20xx

DOI: 10.1039/x0xx00000x

The development of low-cost, highly efficient and stable electrocatalysts for the oxygen evolution reaction (OER) is of great significance in a few promising energy storage and conversion applications, including metal-air batteries and water splitting technology. Herein, layer-structured $Ca_{0.5}CoO_2$ nanofibers made of interconnected ultrathin nanoplates have been successfully synthesized by an electrospinning strategy. The OER activity of the $Ca_{0.5}CoO_2$ can be dramatically improved by iron doping, and the overpotential of the $Ca_{0.5}Co_{1-x}Fe_xO_2$ (x=0.25) is only 346 mV at a current density of 10 mA cm^{-2}. The mass and intrinsic activities of $Ca_{0.5}Co_{0.75}Fe_{0.25}O_2$ at 1.6 V are approximately 18.7 and 11.4 times higher than that of the $Ca_{0.5}CoO_2$. Iron doping modifies the electronic structure of the $Ca_{0.5}CoO_2$ with a partial oxidation of the surface cobalt and an increased amount of highly oxidative active species O_2^{2-}/O_2. Consequently, $Ca_{0.5}Co_{0.75}Fe_{0.25}O_2$ nanofibers with tuned electronic state have shown great potential as cost-effective and efficient electrocatalysts for OER.

1. Introduction

Developing renewable energy is essential to mitigate the growing concern of the energy crisis worldwide [1-4]. However, the practical process in the storage and conversion of sustainable alternatives is often limited by the sluggish chemical reactions [5, 6]. In particular, the bottleneck of hydrogen production in water splitting is the kinetically sluggish oxygen evolution reaction (OER) [7, 8]. Nobel metal oxides of IrO_2 and RuO_2 are currently the superior electrocatalysts for the OER, but their widespread applications are severely limited by the resource deficiency and the noble metal dissolution at high potential [9-11]. Therefore, the rational design of low-cost, efficient and durable alternatives is of great significance but remains a large challenge towards sustainable energy application field.

In the past decade, 3*d* transition metal-based layer-structured materials have drawn an increasing attention as alternative candicates in OER due to their resource abundance and competitive OER activity in comparison to noble IrO_2 and RuO_2 [12, 13]. In particular, a series of $LiCoO_2$-based electrocatalysts has been explored for oxygen electrocatalysis. For instance, $Li_{0.5}CoO_2$ was designed as an efficient catalyst for oxygen evolution reaction [14]. $LiCoO_2$-based electrocatalyst was developed by a combination of Mg doping and shear force-assisted exfoliation strategy [15]. Further, it has been demonstrated that introduction of La breaks the Oh symmetry of the CoO_6 octahedron in $LiCoO_2$, which resulted in its enhanced oxygen evolution activity [16]. However, $LiCoO_2$ as a catalyst suffers from low abundance, high cost, low activity and Li^+ dissociation. In contrast to lithium, calcium with larger ionic radium is relatively abundant in the earth's crust (3th most abundant metallic element) [17]. Thus, $Ca_{0.5}CoO_2$ could be a low-cost alternative to the layer-structured $LiCoO_2$. Nevertheless, in comparison with $LiCoO_2$, Ca-containing layered oxides have been rarely reported as electrocatalysts OER.

Cation doping is proved to be a promising technique for the modification of the transition metal-based electrocatalysts to improve the electrocatalytic activity [18]. In particular, Fe cation has been found as an effective dopant to improve the OER behaviors of transition metal-based catalysts [19]. For instance, the electrocatalytic activities of Ni_2P could be effectively improved by introduction of iron species, indicating the superior iron species-modified electrochemical performance [20]. The Fe-doping was also found to be conducive to optimize the electronic conductivity of $NiSe_2$ and create more active sites due to the heteroatom displacement defects [21]. Fe-doped $Ni(OH)_2$ nanosheets demonstrated modified catalytic performance compared with pristine NiFe LDH and $Ni(OH)_2$, which was attributed to the increased abundant defects and active sites and enhanced surface wettability [22].

In addition to cation doping[21, 23, 24], nanostructure engineering is an effective strategy to enhance the mass activity of catalysts by increasing the exposed electrocatalytic active sites [25]. The combination of composition tuning and nanostructure engineering is expected to result in significantly enhanced electrocatalytic activity [26, 27].

Herein, we have successfully designed layer-structured $Ca_{0.5}CoO_2$ (denoted as CC) nanofibers composed of

[a] Key Laboratory of Groundwater Resources and Environment, Ministry of Education, Jilin University, Changchun, 130021, Jilin, China.
[b] Jilin Provincial Key Laboratory of Water Resources and Environment, Jilin University, Changchun 130021, Jilin, China.
[c] School of Materials Science and Engineering, Georgia Institute of Technology, Atlanta, GA 30332-0245, USA.
[d] School of Environment and Energy, South China University of Technology, Guangzhou 510006, China.
Electronic Supplementary Information (ESI) available: See DOI: 10.1039/x0xx00000x

interconnected ultrathin nanoplates by an electrospinning strategy. The intrinsic and mass activity have been enhanced dramatically with the nanostructure engineering and iron doping [28, 29]. Iron doping modifies the electronic structure of the CC with a partial oxidation of the surface Co^{3+} and the increase of highly reactive oxygen species O_2^{2-}/O_2. In addition, based on the unique nanofiber structure, a high surface area has been achieved with more active sites exposed. These findings endow the active and robust $Ca_{0.5}Co_{0.75}Fe_{0.25}O_2$ with potential as a superior electrocatalyst for OER.

2. Experimental section

2.1 Catalyst synthesis

CC and $Ca_{0.5}Co_{1-x}Fe_xO_2$ (CCFx) nanofibers were synthesized by an electrospinning method followed by an annealing process (x=0.063, 0.125 and 0.25, denoted as CCF0.063, CCF0.125 and CCF0.25, respectively). In a typical process, stoichiometric amounts of $Ca(NO_3)_2{\cdot}4H_2O$ and $Co(NO_3)_2{\cdot}6H_2O$ were dissolved in N, N-dimethylformamide (DMF, 5 mL). After stirring at room temperature for 30 min, PVP powder (1.3 g) and ethanol (5 mL) were added into the above solution, which was further stirred overnight to obtain the uniform precursor solution. The as-prepared solution was transferred into a plastic syringe for electrospinning. The parameters for the electrospinning were as follows: a 27-G needle, a feeding rate of 0.3 mL min^{-1}, an applied voltage of 18 kV, a needle tip to drum collector distance of 15 cm and a relative humidity of 25-35 %. The as-obtained electrospun nanofibers were annealed in air at 650 °C for 3 h with a heating and cooling rate of 1 °C min^{-1} and 3 °C min^{-1}, respectively.

2.2. Material characterization

X-ray diffraction (XRD) patterns were collected with an X'Pert PRO Alpha-1 X-ray diffractometer. The morphologies of as-made catalysts were characterized by a scanning electron microscope (SEM, SU8010, Hitachi) and a high-resolution transmission electron microscope (HRTEM, FEI Tecnai G^2 F30). X-ray photoelectron spectroscopy (XPS) measurement was carried on a Thermo K-Alpha XPS spectrometer equipped with a monochromatic Al-Ka X-ray source (hv=1468.6 eV).

2.3 Electrochemical measurement

The catalyst ink was obtained by mixing of the catalyst (2.0 mg), acetylene black carbon (0.5 mg), Nafion solution (25.0 μL) and deionized water/isopropanol solvent (3:1 (v/v), 1 mL). Before drop-casting, the catalyst ink was sonicated for 1 h to obtain a uniform solution. The ink solution (20 μL) was dropped to the glassy carbon (GC, 5mm in diameter) electrode and fully dried before the measurements. The mass loading of the sample was 0.202 mg cm^{-2}. A conventional three electrode cell system was employed by using a GC electrode as the working electrode, a Pt wire as the counter electrode, an Hg/HgO electrode as the reference electrode and a KOH aqueous solution (1 M) as the electrolyte. And the electrode was saturated with oxygen before the measurements. Electrochemical measurements were carried out on a Solartron electrochemical workstation equipped with a rotating disk electrode (RDE) system (Pine Instrument Company, USA).

To evaluate the OER activity, linear sweep voltammetry (LSV) curves were performed from 0.3 to 0.73 V *vs.* Hg/HgO at a scan rate of 10 mV s^{-1} with a rotation rate of 1600 r min^{-1}. Tafel plots were calculated from the steady-state measurements. Electrochemical Impedance Spectroscopy (EIS) measurements were collected from 100 kHz to 50 mHz at a potential of 0.65 V *vs.* Hg/HgO with 10 mV amplitude. Chronopotentiometric measurements were recorded on working electrode at a current density of 10 mA cm^{-2} for 12 h. All potentials were calibrated with reversible hydrogen electrode (RHE) and corrected with *iR*-compensation.

3. Results and discusstion

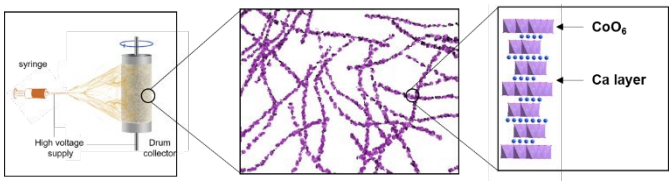

Figure 1. Schematic illustration for the preparation of the CC.

The layer-structured CC nanofibers were synthesized by an electrospinning method (Figure 1). Fe-doped CC nanofibers (i.e., $Ca_{0.5}Co_{1-x}Fe_xO_2$, denoted as CCFx, x = 0.063, 0.125, 0.25 and 0.375) were also prepared in the same fashion.

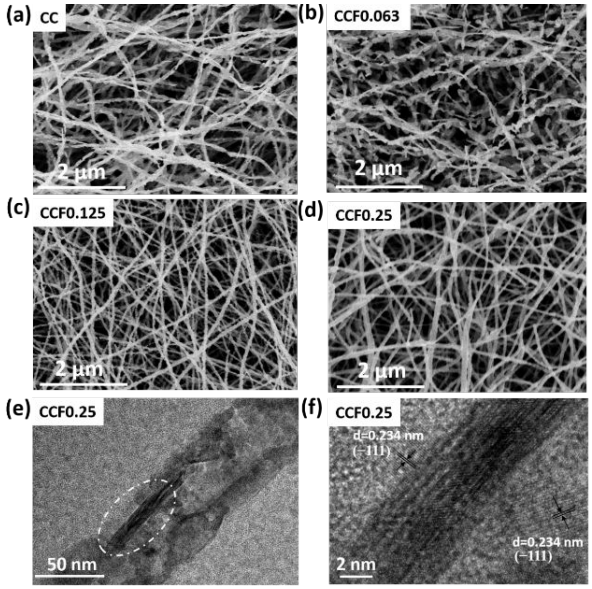

Figure 2. SEM images of (a) CC, (b) CCF0.063, (c) CCF0.125 and (d) CCF0.25. (e) TEM and (f) HRTEM images of the CCF0.25.

Figure 2 shows the SEM images of CCF. All CCF samples doped with different amounts of iron are nanofibers with average diameters of *ca.* 70 nm (Figure S1). Specifically, the $Ca_{0.5}CoO_2$ and $Ca_{0.5}Co_{0.937}Fe_{0.063}O_2$ are nanofiber architecture composed of interconnected nanoplates. With increasing the amount of the doped iron to x=0.125 and 0.25, the morphologies of the $Ca_{0.5}Co_{0.875}Fe_{0.125}O_2$ and $Ca_{0.5}Co_{0.75}Fe_{0.25}O_2$ are still nanofiber structures but composed of nanoparticles (Figure 2c-d).

Elemental mapping in Figure S2 demonstrates the uniform distribution of Ca, Co, Fe and O elements (Table S1).

The TEM analysis indicates that CCF0.25 has discontinuous pores inside (Figures 2e, S3), which were created by the gases released from the decomposition of metal nitride precursors and PVP. The lattice spacing of CCF0.25 was measured to be 0.234 nm by HRTEM (Figure 2f), which is corresponding to the (−111) facet of the $CaCo_2O_4$ crystal, and the HRTEM results are consistent with the XRD patterns. The Brunauer-Emmett-Teller (BET) surface areas are 22.3, 20.8, 31.3 and 35.3 $m^2\ g^{-1}$ for CC, CCF0.063, CCF0.125 and CCF0.25 samples, respectively (Figure S4).

Figure 3 illustrates the XRD patterns of the as-obtained CC and CCFx nanofibers doped with different amounts of iron. Among the samples, the diffraction peaks of the as-synthesized CC and CCF0.063 were in accordance with the standard patterns of the layer-structured $CaCo_2O_4$ (JCPDS No. 51-1760). With further increasing the iron content in CCFx to x= 0.125 and 0.25, some of the diffraction peaks disappeared but no impurity phase was detected. The full width at half maxima (FWHM) of typical peaks was increased and the peak intensity was decreased, which could be attributed to the presence of disordered structure. However, the phase of $CaFe_2O_5$ (JCPDS No. 38-0408) emerged in the pattern of CCF0.375 sample, indicating that the amount of iron doping in the cobalt site should be less than 0.375. Moreover, the XRD results are in accordance with those of the SEM images. Specifically, the CC and CCF0.063 were nanofiber architecture composed of interconnected nanoplates. With increasing the amount of the doped iron to x=0.125 and 0.25, the morphologies of the CCF0.125 and CCF0.25 were still nanofiber structures, but the interconnected nanoplates became smaller. (Figure 2c-d).

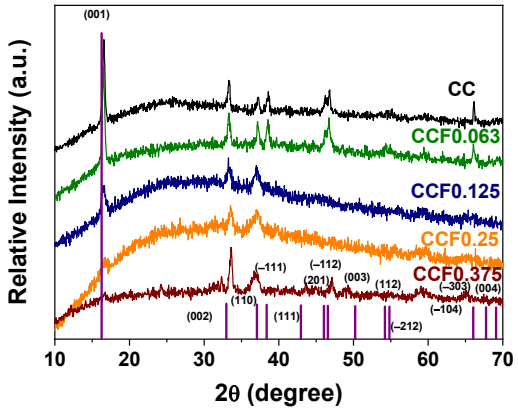

Figure 3. XRD patterns of CC, CCF0.063, CCF0.125, CCF0.25 and CCF0.375.

The OER performance of the as-prepared catalysts was measured with a rotating disk electrode (RDE) system. The catalyst was uniformly drop-casted on a glassy carbon (GC) RDE with the areal mass loading of 0.202 mg cm^{-2} for all samples. The typical *iR*-corrected OER LSV curves are shown in Figure 4a and Figure S5. The CCF0.25 nanofibers exhibit the lowest onset potential and potential (346 mV) at benchmark of 10 mA cm^{-2}_{geo}. The overpotential of the CCF0.25 nanofibers was much lower compared to that of the CC sample (410 mV) at the same current density. Besides, The turnover frequency value of the CC, CCF0.063, CCF0.125 and CCF0.25 was calculated to be 6.0×10^{-4} s^{-1}, 1.2×10^{-3} s^{-1}, 3.0×10^{-3} s^{-1} and 0.02 s^{-1} (Table S1). Moreover, the continuous cyclic voltammetry (CV) measurements manifest that the intial activation of all CC and CCFx electrocatalysts was done after 15 cycles (Figure S6).

Tafel plots were calculated from the steady-state measurements, and the tafel slope of the CCF0.25 is the lowest (39.3 mV dec^{-1}) among the electrocatalysts, indicating that the OER performance and kinetics are co-enhanced by iron doping (Figure 4b). EIS measurements were preformed to obtain the charge transfer resistance (R_{ct}) of the electrocatalysts (Figure 4c). The R_{ct} of CCF0.25 is much smaller than that of CC, CCF0.063 and CCF0.125, indicating the fastest charge transfer capability in the CCF0.25 during OER process. Moreover, the mass loading-normalized kinetic current density (mass activity) of CCF0.25 at 1.6 V (*vs*. RHE) is *ca.*18.7, 6.2 and 3.6 times higher than that of the CC, CCF0.063 and CCF0.125, respectively. And the BET surface area normalized kinetic current density (intrinsic activity) of CCF0.25 at 1.6 V (*vs*. RHE) is *ca.* 11.4, 3.2 and 3.1 times higher than that of the CC, CCF0.063 and CCF0.125, respectively (Figure 4d). The detailed electrocatalytic parameters of the catalysts are summarized in Table S2. Compared with the recently reported electrocatalysts, CCF0.25 nanofibers show a comparable OER activity in terms of *iR*-corrected overpotential, tafel slope and the mass loading in 1 M KOH, suggesting that the CCF0.25 nanofiber is a highly promising electrocatalyst for OER (Table S3).

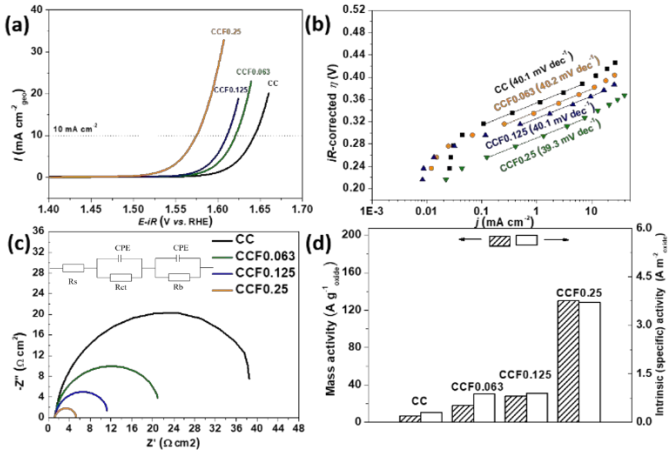

Figure 4. (a) *iR*-corrected OER LSV curves of CC, CCF0.063, CCF0.125 and CCF0.25 nanofibers. (b) Tafel plots calculated by the steady-state measurements. (c) Electrochemical impedance spectra recorded at a constant potential of 1.566 V (*vs*. RHE). (d) Mass activities and intrinsic activities of the electrocatalysts at 1.6 V.

The stability of the CCF0.25 was measured by chronopotentiometry. There are no significant changes in the potential (from 1.57 to 1.58 V) for the CCF0.25 catalyst after test at the current density of 10 mA cm^{-2}_{geo} for 12 h (Figure 5a). The morphology and structure of the CCF0.25 after stability test were also investigated. The electrocatalysts still maintain the

nanofiber structure (Figure S7). The HRTEM image further shows that CCF0.25 nanofibers after stability test still possess the lattice spacing of 0.234 nm, which is in agreement with the (−111) facet of the $CaCo_2O_4$ crystal (Figure 5b). The HRTEM results are consistence with the results of the as-prepared samples (Figure 2e-f).

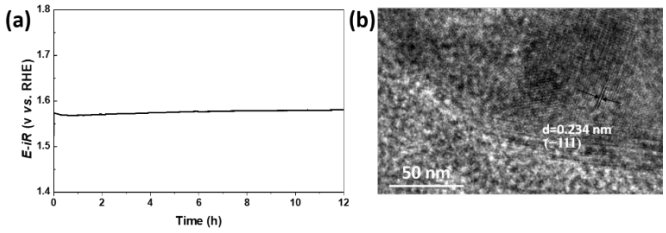

Figure 5. (a) *iR*-corrected chronopotentiometry curve of CCF0.25 nanofibers at a constant current density of 10 mA cm^{-2}_{geo}. (b) HRTEM image of the CCF0.25 after stability test for 12 h.

XPS characterization was further executed to explore the information of the surface electronic states in the CC and CCF nanofibers (Figure 6). Both the XPS survey spectra of CC and CCF0.25 (Figure 6a) confirm the existence of the Ca, Co and O. However, some differences still exist in the peaks from 710 eV to 720 eV, which are corresponding to Co Auger in CC and Fe 2p in CCF0.25, respectively. High-resolution Co 2p XPS spectra was also measured in CC and CCF0.25 samples (Figure 6b). Compared with CC, a lower satellite (sat) peak was observed in CCF0.25. A higher binding energy of main peak and broader FWHM were observed in Co 2p spectra, indicating the partial oxidation of surface Co in CCF0.25 (Figure S8). The Co $2p_{3/2}$ peak of the as-maded CC and CCF0.25 catalyst indicates that Co exists mainly in the form of octahedral Co^{3+} (779.6 eV) with a minor portion of tetrahedral Co^{2+} (781.5 eV), and the ratio of Co^{3+} has been increased in CCF0.25. [30]. The positive shift of the Co 3p main peak and the decrease of satellite peak area manifest the oxidation process of Co^{3+}. Moreover, both peaks of the Co 3p and Co 3s show the positive shift and obvious broadening in CCF0.25, which further confirm the partial oxidation of surface Co and the weak splitting of Co, respectively (Figure S9). In contrast, the peaks of Fe $2P_{3/2}$ show a lower binding energy shift (Figure S10). It has been reported that cobalt cations with high valence state are beneficial to the OER[15, 31], as Co with a high valance state facilitates the adsorption and further reaction of OH^- to form metal-OOH species [15, 31], which contributes to the enhanced performance of CCF0.25.

High-resolution O 1s spectra show that all the spectra of CC and CCFx can be split into four well-defined peaks, which is in correspondence with the surface-adsorbed molecular water (H_2O, 532.2 eV), adsorbed oxygen or the hydroxyl groups (O_2/–OH, 531.2 eV), highly active species (O_2^{2-}/O^-, 529.8 eV) and lattice oxygen species (O^{2-}, 529.3 eV), respectively (Figure 6c) [31, 32]. The molar fraction of different oxygen species was evaluated from the relative peak area. The result demonstrates that O_2^{2-}/O^- species in CCF0.25 (38.9%) is larger than that in CC (11.3%), which could be attributed to a higher OER activity of CCF0.25, as it has been reported that O_2^{2-}/O^- intermediates produced on the surface of the electrocatalysts are active species for OER [33, 34]. Besides, with increasing the amount of iron dopant, the relative content of the O_2^{2-}/O^- has increased dramatically, which demonstrates the electronic structure regulation after iron doping. The results of highly reactive oxygen species are in accordance with that in high-resolution Co spectra [31].

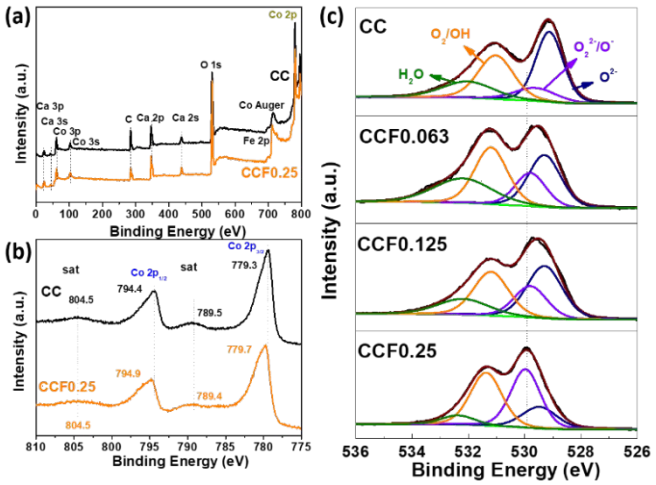

Figure 6. (a) XPS survey spectra and (b) XPS spectra of Co 2p in the CC and CCF0.25. (c) XPS spectra of O 1s species in CC, CCF0.063, CCF0.125 and CCF0.25 nanofibers.

Conclusions

In summary, we have successfully designed a series of layer-structured CC and CCFx nanofibers composed of interconnected ultrathin nanoplates or nanoparticles by electrospinning strategy. By tailoring the nanofiber structure, the surface area has been increased with more active sites exposed. With the introduction of iron dopant in CC, the OER activity of the CCFx can be dramatically enhanced. The mass and intrinsic activities of CCF0.25 are *ca.*18.7 and 11.4 times higher than that of the original CC at 1.6 V. Among the CC and CCFx nanofibers, the overpotential of CCF0.25 is only 346 mV at 10 mA cm^{-2}. Iron doping results in the electronic structure change of the CC with a partial oxidation of the surface Co and the formation of highly reactive oxygen species O_2^{2-}/O_2. These results not only demonstrate that CCF0.25 is a highly efficient and durable OER electrocatalyst, but also pave a promising way for the development of robust OER catalysts with proper doping and tailored nanostructure.

Author Contributions

Mingyu Li: Writing – original draft. Bote Zhao: Methodology, Conceptualization. Yun Zhao: Investigation. Resources. Yu Chen: Validation. Meilin Liu: Supervision.

Conflicts of interest

There are no conflicts to declare.

Acknowledgements

This work was financially supported by the National Natural Science Foundation of China (52100087, 52102248), Natural Science Foundation of Chongqing, China (cstc2021jcyj-msxmX0954). This work was also financially supported by the US National Science Foundation under award number DMR-1742828. M. Y. L. acknowledges the financial support of a scholarship from the China Scholarship Council (CSC).

References

1. J. Xu, T. Liu, J. Li, Y. Liu, B. Zhang, D. Xiong, I. Amorim, W. Li and L. Liu, *Energy Environ Sci*, 2018, **11**, 1819-1827.
2. J. Mahmood, F. Li, S.-M. Jung, M. S. Okyay, I. Ahmad, S.-J. Kim, N. Park, H. Y. Jeong and J.-B. Baek, *Nat Nanotechnol*, 2017, **12**, 441-446.
3. S. Li, Y. Gao, N. Li, L. Ge, X. Bu and P. Feng, *Energy Environ Sci*, 2021, **14**, 1897-1927.
4. Z. L. Zhao, Q. Wang, X. Huang, Q. Feng, S. Gu, Z. Zhang, H. Xu, L. Zeng, M. Gu and H. Li, *Energy Environ Sci*, 2020, **13**, 5143-5151.
5. Y. Xiong, Y. Yang, X. Feng, F. J. DiSalvo and H. D. Abruña, *J Am Chem Soc*, 2019, **141**, 4412-4421.
6. H. A. Tahini, X. Tan, U. Schwingenschlögl and S. C. Smith, *ACS Catalysis*, 2016, **6**, 5565-5570.
7. J. Suntivich, K. J. May, H. A. Gasteiger, J. B. Goodenough and Y. Shao-Horn, *Science*, 2011, **334**, 1383-1385.
8. L. C. Seitz, C. F. Dickens, K. Nishio, Y. Hikita, J. Montoya, A. Doyle, C. Kirk, A. Vojvodic, H. Y. Hwang, J. K. Norskov and T. F. Jaramillo, *Science*, 2016, **353**, 1011-1014.
9. J. Liu, Y. Ji, J. Nai, X. Niu, Y. Luo, L. Guo and S. Yang, *Energy Environ Sci*, 2018, **11**, 1736-1741.
10. Q. Ji, C. Li, J. Wang, J. Niu, Y. Gong, Z. Zhang, Q. Fang, Y. Zhang, J. Shi, L. Liao, X. Wu, L. Gu, Z. Liu and Y. Zhang, *Nano Lett*, 2017, **17**, 4908-4916.
11. O. Kasian, S. Geiger, T. Li, J. P. Grote, K. Schweinar, S. Y. Zhang, C. Scheu, D. Raabe, S. Cherevko, B. Gault and K. J. J. Mayrhofer, *Energy Environ Sci*, 2019, **12**, 3548-3555.
12. H. Zhu, J. Zhang, R. Yanzhang, M. Du, Q. Wang, G. Gao, J. Wu, G. Wu, M. Zhang, B. Liu, J. Yao and X. Zhang, *Adv Mater*, 2015, **27**, 4752-4759.
13. M. Qin, S. Li, Y. Zhao, C.-Y. Lao, Z. Zhang, L. Liu, F. Fang, H. Wu, B. Jia, Z. Liu, W. Wang, Y. Liu and X. Qu, *Adv Energy Mater*, 2019, **9**, 1970003.
14. Z. Lu, H. Wang, D. Kong, K. Yan, P.-C. Hsu, G. Zheng, H. Yao, Z. Liang, X. Sun and Y. Cui, *Nat Commun*, 2014, **5**, 4345.
15. X. Zheng, Y. Chen, X. Zheng, G. Zhao, K. Rui, P. Li, X. Xu, Z. Cheng, S. X. Dou and W. Sun, *Adv Energy Mater*, 2019, **9**, 1803482.
16. Z. R. Zhang, C. X. Liu, C. Feng, P. F. Gao, Y. L. Liu, F. N. Ren, Y. F. Zhu, C. Cao, W. S. Yan, R. Si, S. M. Zhou and J. Zeng, *Nano Lett*, 2019, **19**, 8774-8779.
17. J. G. Lee, J.-H. Myung, A. B. Naden, O. S. Jeon, Y. G. Shul and J. T. S. Irvine, *Advanced Energy Materials*, 2020, **10**, 1903693.
18. Y. Li, F.-M. Li, X.-Y. Meng, X.-R. Wu, S.-N. Li and Y. Chen, *Nano Energy*, 2018, **54**, 238-250.
19. M. Li, Y. Gu, Y. J. Chang, X. C. Gu, J. Q. Tian, X. Wu and L. G. Feng, *Chem Eng J* 2021, **425**, 130686.
20. H. Huang, C. Yu, C. Zhao, X. Han, J. Yang, Z. Liu, S. Li, M. Zhang and J. Qiu, *Nano Energy*, 2017, **34**, 472-480.
21. J. Zhou, L. Yuan, J. Wang, L. Song, Y. You, R. Zhou, J. Zhang and J. Xu, *Journal of Materials Chemistry A*, 2020, **8**, 8113-8120.
22. Q. Zhou, Y. Chen, G. Zhao, Y. Lin, Z. Yu, X. Xu, X. Wang, H. K. Liu, W. Sun and S. X. Dou, *Acs Catalysis*, 2018, **8**, 5382-5390.
23. J. M. P. Martirez and E. A. Carter, *J Am Chem Soc*, 2019, **141**, 693-705.
24. S. Zhang, B. Huang, L. Wang, X. Zhang, H. Zhu, X. Zhu, J. Li, S. Guo and E. Wang, *ACS Applied Materials & Interfaces*, 2020, **12**, 40220-40228.
25. M.-Q. Wang, C. Ye, H. Liu, M. Xu and S.-J. Bao, *Angew Chem Int Ed*, 2018, **57**, 1963-1967.
26. B. Zhao, L. Zhang, D. Zhen, S. Yoo, Y. Ding, D. Chen, Y. Chen, Q. Zhang, B. Doyle, X. Xiong and M. Liu, *Nat Commun*, 2017, **8**, 14586.
27. C. Lv, J. Sun, G. Chen, Y. Zhou, D. Li, Z. Wang and B. Zhao, *Applied Catalysis B: Environmental*, 2017, **208**, 14-21.
28. Y. L. Zhu, W. Zhou, Z. G. Chen, Y. B. Chen, C. Su, M. O. Tade and Z. P. Shao, *Angew Chem Int Ed*, 2015, **54**, 3897-3901.
29. S. Zhou, X. Miao, X. Zhao, C. Ma, Y. Qiu, Z. Hu, J. Zhao, L. Shi and J. Zeng, *Nat Commun*, 2016, **7**, 11510.
30. X. Han, C. Yu, S. Zhou, C. Zhao, H. Huang, J. Yang, Z. Liu, J. Zhao and J. Qiu, *Adv Energy Mater*, 2017, **7**, 1602148.
31. Y. Zhu, W. Zhou, Y. Chen, J. Yu, M. Liu and Z. Shao, *Adv Mater*, 2015, **27**, 7150-7155.
32. J. Dai, Y. Zhu, Y. Chen, W. Zhou and Z. Shao, *ACS Applied Materials & Interfaces*, 2017, **9**, 21587-21592.
33. R. Liu, F. Liang, W. Zhou, Y. Yang and Z. Zhu, *Nano Energy*, 2015, **12**, 115-122.
34. J. I. Jung, H. Y. Jeong, J. S. Lee, M. G. Kim and J. Cho, *Angew Chem Int Ed*, 2014, **53**, 4582-4586.